Inertial measurements processing for sway angle estimation in overhead crane control applications

Václav Helma[1], Martin Goubej[2] and Vlastimil Šetka[3]

***Abstract*— The main scope of this paper is to propose data fusion algorithms suitable for estimation of gantry crane hook tilt angles based on the MEMS accelerometer and gyroscope readings. Such methods should merge useful information from both these sensors into a better estimate than those based on the measurement from the single device. In the first place, these algorithms should deal with the typical measurement noise which the MEMS readings are known to suffer from. Besides these errors, also the impact of the angular acceleration caused by the crane hook motion and translational acceleration due to cart motion distorting the gravitational vector sensing should be taken into account when designing the data fusion algorithm. The presented methods will be compared by means of experimental tests using a wireless inertial measurement unit developed at our workplace. The goal is to verify practical viability of the algorithms aiming at delivery of tilt angles information which may be used in an active anti-sway stabilization system.**

I. Introduction

Crane systems are used extensively for pick-and-place operations in various application domains ranging from construction, factory automation to assembly or ship cargo transfer. A fundamental difficulty with unwanted motion- or disturbance-induced oscillations of the hanging load inherently comes from the underactuated dynamics of the crane. Extensive research is devoted to the development of intelligent control systems allowing either full automation of the motion tasks or at least providing assistance to a human operator.

Crane control is now a well-established research field and several approaches with regards to load sway problem were proposed in the last few decades. They can be classified into two main groups as passive (or feedforward) and active (feedback) methods. The passive approach is to modify the trajectory of the hoist drive in such a way that the oscillatory modes of the system are not excited. Input shaping filters or input-output inversion techniques have been used extensively for this purpose [1]–[5]. On the other hand, active methods employ a feedback compensator which enforce a well-damped closed-loop dynamics by means of a proper load-sway sensor. Several control strategies were proposed in the literature ranging from classical PID [6] or LQR/LQG control [7] to model-predictive [8], sliding-mode [9] or nonlinear and adaptive control algorithms [10], [11].

All the authors are with NTIS Research Centre, University of West Bohemia, Pilsen, Czechia

[1] helma@ntis.zcu.cz

[2] mgoubej@ntis.zcu.cz

[3] setka@ntis.zcu.cz

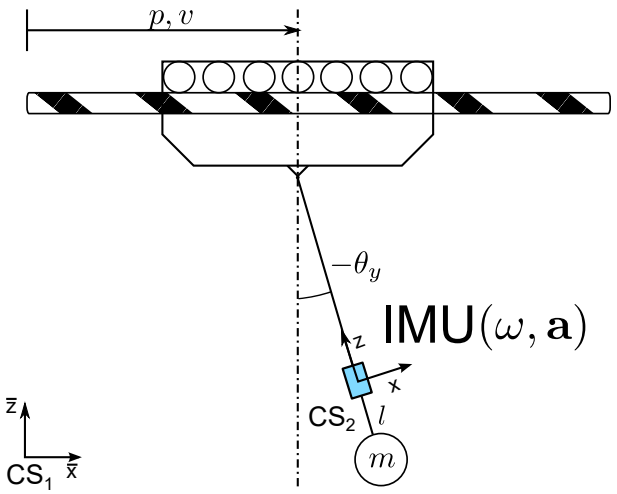

Fig. 1. Problem formulation - reconstruction of the load-sway angle θ in the global coordinate system CS_1 from the inertial measurement unit providing angular rates ω and accelerations $\mathbf{a}$ in the local coordinate system CS_2 of the load-attached sensor, p, v denotes hoist position and velocity

An extensive survey of crane control methods is given in [12].

The feedback approach comes with a significant advantage of active disturbance rejection capability. This may be relevant for cranes operating outdoors that are subject to the environmental effects. A fundamental problem is to detect the load-side motion correctly by means of a proper sensory system in order to supply the information to the feedback controller. The load-side motion can be estimated indirectly by observing the hoist behaviour and using a dynamical crane model [13], [14]. This avoids the necessity of installation of complex instrumentation at the cost of performance degradation because of the lack of direct load-side measurement. A commonly used direct approach is to use an optical image sensor [15]–[19] which, complemented by advanced signal processing algorithms, can provide high-fidelity feedback information. High cost and sensitivity to environmental conditions should be considered as potential drawbacks. As an alternative, cheaper sensory systems were proposed including laser sensors [20], inclinometers [21], accelerometers [13], gyroscopes [22] or special-purpose devices [23] providing cost-efficient and robust solution. With the recent advances in MEMS technology, utilization of inertial measurement units (IMUs) combining multi-axis acceleration and angular rate sensors in one compact package seems to be a viable way of implementing the feedback system. The IMUs are routinely used in the field of unmanned aerial vehicles to deliver attitude information to the flight controller. Various data-

fusion algorithms were proposed to combine the readings from accelerometers, gyros and eventually magnetometers in order to improve the overall motion sensing accuracy [24]–[26]. They can be, in principle, used in the same manner in crane systems for the load sway measurement. However, practical experience shows that severe performance deterioration can occur because of the large translational accelerations which deflect the gravity vector sensed by the accelerometer sensor in steady state and cause a systematic error when not treated properly. The goal of the paper is to provide a data-fusion algorithm suitable for the estimation of the load tilt angles and their derivatives by combining the raw IMU data with the dynamic model of the plant.

The paper is organized as follows. Section II deals with the description of the proposed algorithms. Section III presents experimental results achieved with a small-scale crane model and a proprietary wireless sensory system developed at our workplace. Concluding remarks are given in the last part.

II. Algorithms

In this section, two distinct algorithms dealing with the tilt angle estimation are described. Both these methods adopt the Extended Kalman filter (EKF) for angle estimation. However, they differ in the problem formulation.

First, a modification of a standard algorithm [27] tailored to the single angle estimation is presented (i.e. we consider the rotation about a single axis which is the case of a single axis crane). However, as it turns out, this method is not appropriate for the application of pendulum (gantry crane) sway angle estimation since such a formulation does not consider the acceleration contributions from rotational pendulum motion and cart translational motion into the total IMU reference frame acceleration which is expected to be measured by the accelerometer. For this reason, such an approach may produce misleading and incorrect estimate. This was the motivation for the development of a pendulum-on-cart model-based algorithm.

The proposed method employs a pendulum and cart velocity-loop model in the state equations and maps the output equations to the IMU measurements. This allows to include all the expected contributions from the acceleration caused by pendulum and cart motion, which is the major difference to the standard algorithm mentioned previously. Besides the improved angle estimate accuracy, the algorithm provides also the estimated angular velocity of the pendulum which is needed e.g. for a full-state feedback control. The latter property of the proposed method is desirable because we get smoothed angular velocity estimate without having to rely on the noisy gyroscope readings that could cause troubles in the control algorithm itself (e.g. a necessary restriction of the closed-loop bandwidth due to noise amplification).

In the following text, the state-space problem formulation of the two aforementioned approaches is given followed by the outline of the EKF algorithm which gives a common framework for both methods.

A. Problem formulation

1) Standard tilt angle estimation - Algorithm 1: In this case, the state equation is given simply as

$$\dot{x}(t) = f_{a1}(\omega_y(t)) = \omega_y(t), \tag{1}$$

with $x(t) = \hat{\theta}_y(t)$ the estimated tilt angle and $\omega_y(t)$ the gyroscope measurement of the angular velocity about the y-axis (Fig. 1).

The output equations can be obtained by transforming the gravitational acceleration vector (with the magnitude g) from the world frame of reference to the IMU coordinate system (provided that for $\hat{\theta}_y(t) = 0$ all the axis of both reference frames are perfectly aligned) resulting in

$$\vec{y}(t) = h_{a1}(x(t)) = \begin{bmatrix} -sin(x(t))g \\ cos(x(t))g \end{bmatrix}, \tag{2}$$

where $\vec{y}(t) = [\hat{g}_x(t), \hat{g}_z(t)]^T$ is the expected projection of the gravitational acceleration vector to the x- and z-axis of IMU reference frame (CS_2 in Fig. 1). This generally corresponds to the accelerometer measurements only if no translational and angular acceleration of the IMU is assumed.

The measurement vector needed for the update in the EKF algorithm is then considered as $\vec{z}(t) = [a_x(t), a_z(t)]^T$ with $a_x(t)$ and $a_z(t)$ designating the accelerometer measurements in x- and z-axis respectively.

2) Formulation based on pendulum-on-cart model - Algorithm 2: We will assume the undamped pendulum motion described by differential equation

$$\ddot{\theta}_y(t) = \frac{g}{l} sin(\theta_y(t)) + \frac{1}{l}\dot{v}(t) cos(\theta_y(t)), \tag{3}$$

with l denoting the perpendicular distance from the pendulum axis of rotation to the pendulum center of gravity and $v(t)$ being the cart velocity along the $\overline{x}$-axis of the global reference frame (CS_1 in Fig. 1).

The state equation of this formulation can be now obtained by modification of (1) in these respects:

1) The state variable representing the estimate of angular velocity $\hat{\omega}_y(t)$ is added by utilizing (3).
2) The state equations are extended by another variable representing the cart velocity along the x-axis. This state equation realizes the cart velocity loop needed for the practical implementation. The velocity loop dynamics is approximated by a first-order lag described by a time constant τ and static gain K_s.
3) The gyroscope measurement $\omega_y(t)$ is replaced by the angular velocity estimate $x_2(t) = \hat{\omega}_y(t)$ in the state equations.

The state equations then have a form

$$\begin{aligned} \dot{\vec{x}}(t) &= \begin{bmatrix} \dot{x}_1(t) \\ \dot{x}_2(t) \\ \dot{x}_3(t) \end{bmatrix} = f_{a2}(\vec{x}(t), v_{sp}(t)) \\ &= \begin{bmatrix} x_2(t) \\ \frac{K_s c_1 v_{sp}(t) + g s_1 \tau - c_1 x_3(t)}{\tau l} \\ -\frac{1}{\tau} x_3(t) + \frac{K_s}{\tau} v_{sp}(t) \end{bmatrix}, \end{aligned} \tag{4}$$

with $x_1(t) = \hat{\theta}_y(t)$, $x_2(t) = \hat{\omega}_y(t)$ and $x_3(t) = \hat{v}(t)$. To shorten the equations we introduce the notation $c_1 \triangleq cos(x_1(t))$ and $s_1 \triangleq sin(x_1(t))$.

The output equations are given as

$$\vec{y}(t) = h_{a2}(\vec{x}(t), v_{sp}(t)) = \begin{bmatrix} x_2(t) \\ -\frac{K_s c_1 l v_{sp}(t) - K_s c_1 r v_{sp}(t) + g s_1 \tau l - s_1 g r \tau - c_1 l x_3(t) + c_1 r x_3(t)}{\tau l} \\ -\frac{x_2(t)^2 r \tau + K_s s_1 v_{sp}(t) - c_1 g \tau - s_1 x_3(t)}{\tau} \\ x_3(t) \end{bmatrix} \tag{5}$$

where $\vec{y}(t) = [\hat{\omega}_y(t), \hat{a}_x(t), \hat{a}_z(t), \hat{v}(t)]^T$ and r is the perpendicular distance from the pendulum axis of rotation to the position of the IMU which does not necessarily have to be the same as the pendulum length l, i.e. the distance from the pendulum axis of rotation to the pendulum center of gravity. The first element of the vector is the expected gyroscope measurement. The second element is the x-axis acceleration affecting the accelerometer attached to the pendulum and it is given as a sum of three contributions:

- x-axis projection of the gravitational acceleration vector,
- the tangential component of the angular acceleration,
- the x-axis projection of the cart acceleration.

The third element of the vector is analogously the z-axis acceleration expected to be measured by the accelerometer and can be obtained as a sum of three contributions:

- z-axis projection of the gravitational acceleration vector,
- the centripetal component of the angular acceleration,
- the z-axis projection of the cart acceleration.

Finally, the fourth element of the vector $\vec{y}(t)$ is the expected cart velocity.

The measurement vector needed for the update in the EKF algorithm is then considered as $\vec{z}(t) = [\omega_y(t), a_x(t), a_z(t), v(t)]^T$ with $\omega_y(t)$ giving the gyroscope measurement, $a_x(t)$ and $a_z(t)$ denoting the accelerometer measurements in x- and z-axis respectively and $v(t)$ being the measured cart velocity.

B. Extended Kalman filter

Now, the nonlinear filtering problem has to be solved to merge the useful information from the model and the measurements. For this purpose, a standard choice is to employ an Extended Kalman filter to be further introduced.

The state-space models described by state equations (1, 4) and output equations (2, 5) can be discretized by some appropriate method (e.g. Euler method) and extended by the stochastic part (describing the measurement or model uncertainty) leading to

$$\vec{x}_k = f(\vec{x}_{k-1}, \omega_{yk-1}, v_{spk-1}, \vec{w}_{k-1}), \tag{6}$$

$$\vec{y}_k = h(\vec{x}_k, \omega_{yk}, v_{spk}) + \vec{v}_k \tag{7}$$

where $\vec{w}_k$ and $\vec{v}_k$ is considered to be zero-mean Gaussian random noise with covariance matrices $\mathbf{Q}$ and $\mathbf{R}$. The EKF algorithm is usually formally divided into two separate steps called prediction and update.

In prediction step, we determine the a priori estimate $\hat{\vec{x}}_{k|k-1}$ and a priori error covariance matrix $\mathbf{P_{k|k-1}}$ using the model dynamics from equations

$$\begin{aligned} \hat{\vec{x}}_{k|k-1} &= f(\hat{\vec{x}}_{k-1|k-1}, \omega_{yk-1}, v_{spk-1}), \\ \mathbf{F_{k-1}} &= \left.\frac{\partial f}{\partial \vec{x}_{k-1}}\right|_{\hat{\vec{x}}_{k-1|k-1}, \omega_{yk-1}, v_{spk-1}}, \\ \mathbf{L_{k-1}} &= \left.\frac{\partial f}{\partial \vec{w}_{k-1}}\right|_{\hat{\vec{x}}_{k-1|k-1}, \omega_{yk-1}, v_{spk-1}}, \\ \mathbf{P_{k|k-1}} &= \mathbf{F_{k-1}} \mathbf{P_{k-1|k-1}} \mathbf{F_{k-1}}^T + \mathbf{L_{k-1}} \mathbf{Q} \mathbf{L_{k-1}}^T. \end{aligned} \tag{8}$$

In update step, we use the output equations and measurement vector $\vec{z}_k$ to calculate the Kalman gain $\mathbf{K_k}$, a posteriori estimate $\hat{\vec{x}}_{k|k}$ and a posteriori error covariance matrix $\mathbf{P_{k|k}}$ as follows

$$\begin{aligned} \mathbf{H_k} &= \left.\frac{\partial h}{\partial \vec{x}_k}\right|_{\vec{x}_k, \omega_{yk}, v_{spk}}, \\ \mathbf{K_k} &= \mathbf{P_{k|k-1}} \mathbf{H_k^T} \left(\mathbf{H_k} \mathbf{P_{k|k-1}} \mathbf{H_k^T} + \mathbf{R}\right)^{-1}, \\ \hat{\vec{x}}_{k|k} &= \hat{\vec{x}}_{k|k-1} + \mathbf{K_k} \left(\vec{z}_k - h(\hat{\vec{x}}_{k|k-1}, \omega_{yk}, v_{spk})\right), \\ \mathbf{P_{k|k}} &= \mathbf{P_{k|k-1}} - \mathbf{K_k} \mathbf{H_k} \mathbf{P_{k|k-1}}. \end{aligned} \tag{9}$$

III. Experimental results

A pendulum on a cart system (Fig. 9) was used as a small-scale model simulating the gantry crane dynamics. For the experiments, the IMU was attached to the pendulum and the acquired raw data were transmitted to the controller via a wireless communication with 10 ms sampling rate. The moving cart is driven by a linear motor with a high-precision position sensor (1 um resolution). The pendulum arm angle is measured by an incremental rotary encoder (IRC, 0.001° resolution). All the sensors are connected to a single controller unit [28] equipped with the REXYGEN control software [29]. More details about the instrumentation can be found in [30].

By this arrangement, we were able to acquire "true" reference values of the pendulum angle and cart position from very precise encoders and measured raw values from the IMU sampled at the sychronized time instants which allows direct evaluation of the estimators performance. The data fusion algorithms to process the data obtained from IMU were then run offline in MATLAB environment and the results were compared with the reference values.

The system was excited by the velocity set-point $v_{sp}(t)$ which is displayed at the top of Fig. (2) together with the measured velocity $v(t)$. The corresponding pendulum angle $\theta_y(t)$ (the reference value obtained from IRC) is then shown in the bottom part of the Figure. The respective accelerometer and gyroscope measurement can be seen in Fig. 3. The data from IMU are received with a period that is ten times larger than the control period (1 ms velocity-control loop). Therefore, the update step of EKF is performed once per ten prediction steps and for the *Algorithm 1* the gyroscope measurement is held constant in the prediction until the new value is received. The model parameters were determined as

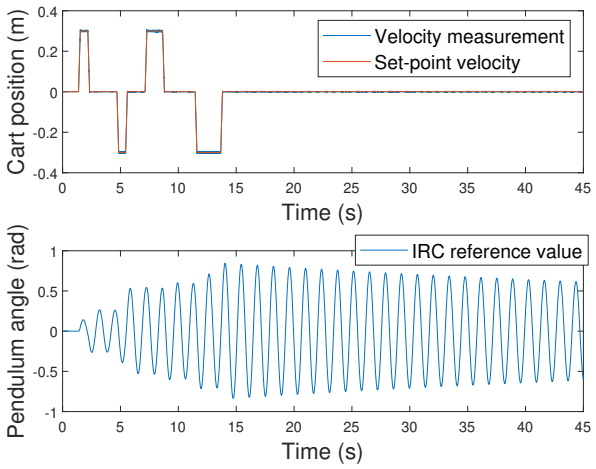

Fig. 2. Experimental data - reference values

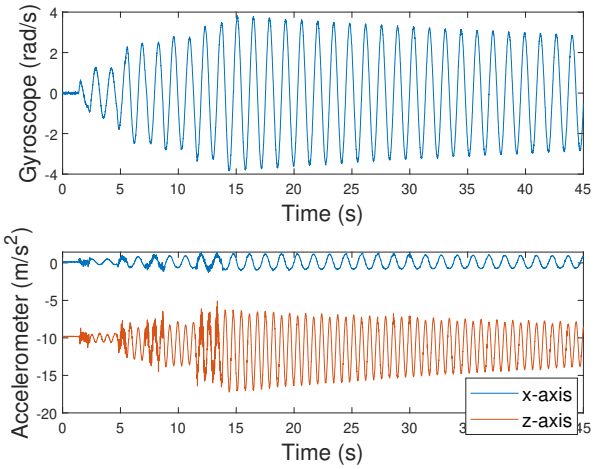

Fig. 3. Experimental data - raw IMU measurements

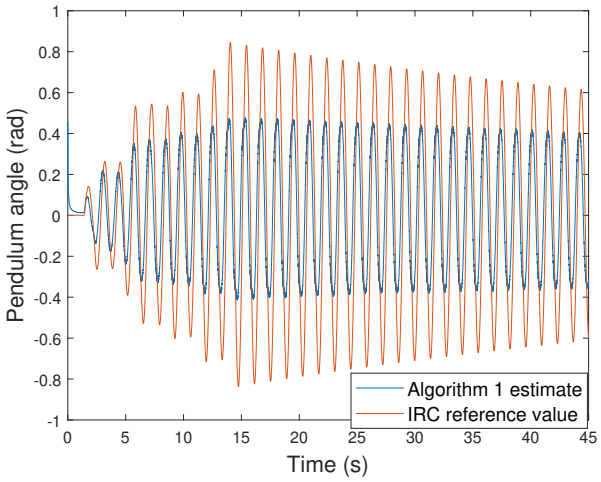

Fig. 4. Algorithm 1 with Setting 1

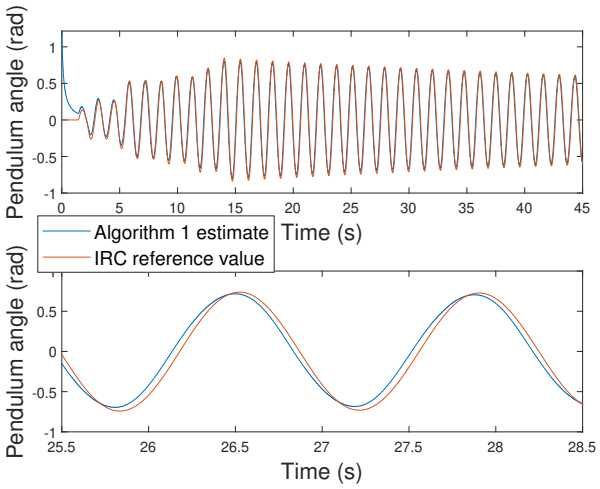

Fig. 5. Algorithm 1 with Setting 2

$l = 0.41\ m$, $r = 0.47\ m$, $g = 9.81\ m/s^2$, $K_s = 1$ and $\tau = 0.002$.

First, *Algorithm 1* was run with the initial value $\hat{\vec{x}}_{0|-1} = 1.3$, initial state error variance $\mathbf{P_{k|-1}} = 0.01$ and the covariance matrices

$$\mathbf{Q} = 0.0011, \quad \mathbf{R} = \begin{bmatrix} 6.94 \cdot 10^{-4} & 4.82 \cdot 10^{-5} \\ 4.82 \cdot 10^{-5} & 4.45 \cdot 10^{-4} \end{bmatrix} \tag{10}$$

statistically estimated from the gyroscope and accelerometer measurements (we will denote this as *Setting 1*). Such a choice of the covariance matrices corresponds to the actual physical interpretation of the measurement noises. The comparison of the pendulum angle estimate $\hat{\theta}_y(t)$ with the reference value $\theta_y(t)$ is shown in Figure 4. We can observe quite poor performance of the estimate which clearly does not track the reference value well, giving a significant error in both phase and amplitude.

Better results in terms of the estimation error can be achieved with a different choice of matrices $\mathbf{Q}$ and $\mathbf{R}$. However, these matrices have no longer a clear physical interpretation and their appropriate setting is a matter of designer intuition. Among all the settings of $\mathbf{Q}$ and $\mathbf{R}$ we tried, the best results were achieved for $\mathbf{Q} = 1$ and $\mathbf{R} = 10 \cdot \mathbf{I}$ (hereafter denoted as *Setting 2*) where $\mathbf{I}$ is the identity matrix. Figure 5 shows the comparison of the estimated angle $\hat{\theta}_y(t)$ with the reference value $\theta_y(t)$ which are also displayed in detail between times $t_1 = 25.5s$ and $t_2 = 28.5s$.

Further, *Algorithm 2* was applied to the measured data with the initial state error $\mathbf{P_{k|-1}} = 0.01 \cdot \mathbf{I}$, the output covariance matrix $\mathbf{R}$ statistically estimated from the gyroscope and accelerometer measurements and the state covariance matrix having a form of $\mathbf{Q} = q \cdot \mathbf{I}$. For convenience, the free parameters (i.e. elements of matrix $\mathbf{Q}$) were reduced to one user parameter q which can be interpreted as a measure of model confidence (i.e. how much we trust the model).

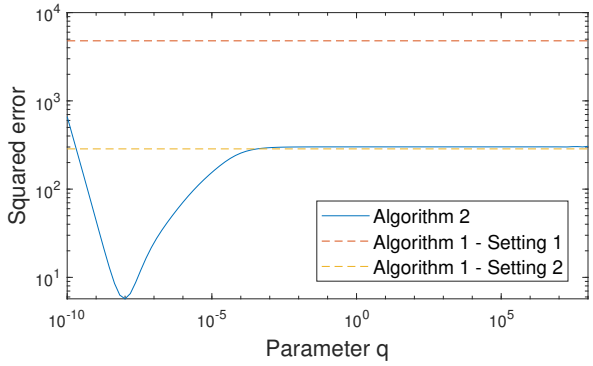

Fig. 6. Squared error - comparison

A sum of squared errors of the angle estimates is introduced as

$$J = \sum_{k=1}^{N} (\hat{\theta}_y(k) - \theta_y(k))^2, \tag{11}$$

where $\hat{\theta}_y(k)$ and $\theta_y(k)$ for $k = 1, \ldots, N$ are the sequences of the pendulum angle estimate and the reference value respectively. Fig. 6 shows the squared error J achieved by *Algorithm 2* as a function of the user parameter q denoted by the solid blue line. The dashed lines then belong to the values of J achieved by *Algorithm 1* with *Setting 1* and *Setting 2*. Note that in this case the algorithms were run from the initial conditions $\vec{\hat{x}}_{0|-1} = [0\ 0\ 0]^T$ and $\vec{\hat{x}}_{0|-1} = 0$ respectively in order to avoid the transient effect at the beginning that could distort the squared error value. It can be observed that by using *Algorithm 2* we are able to achieve better or at least equal performance (evaluated by the squared error J) compared to the case when employing *Algorithm 1* for a wide range of parameters q. Moreover, with the proper choice of parameter q a significant improvement can be obtained, reducing the error in the order of two to three magnitudes.

Next, *Algorithm 2* was applied to the measured data with the initial value $\vec{\hat{x}}_{0|-1} = [1.3\ 0\ 0]^T$, initial state error $\mathbf{P_{k|-1}} = 0.01 \cdot \mathbf{I}$, the output covariance matrix $\mathbf{R}$ statistically estimated from the gyroscope and accelerometer measurements and the state covariance matrix having a form $\mathbf{Q} = q \cdot \mathbf{I}$ with q set as the optimal value obtained from Fig. 6, i.e. $q = 1 \cdot 10^{-8}$. Fig. 7 shows the time plot of the estimated pendulum angle obtained by *Algorithm 2* in comparison with the reference value and also with the estimate achieved by *Algorithm 1* with *Setting 2*. Figure 7 confirms that by employing *Algorithm 2* we can achieve a significant performance enhancement compared to the case when using *Algorithm 1*.

The *Algorithm 2* provides also the estimated angular velocity of the pendulum which is shown in Fig. 8 in comparison with the gyroscope measurement. Advantageously, the filter results in smoothed angular velocity estimates which are more suitable for feedback control applications than the raw readings from gyros. Potential problems with propagation of the measurement noise into the control action as well as

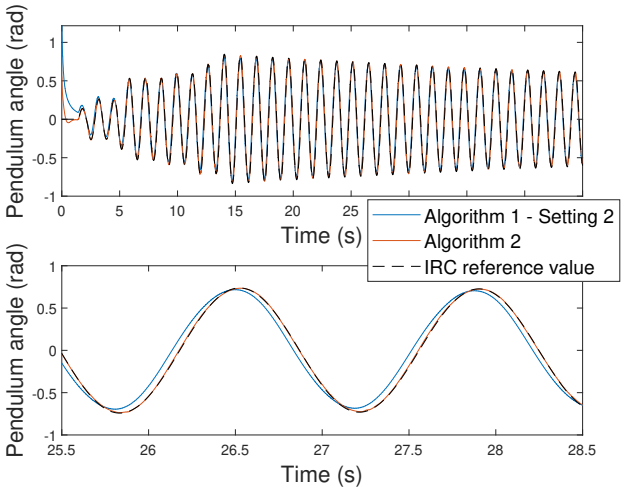

Fig. 7. Algorithm 2

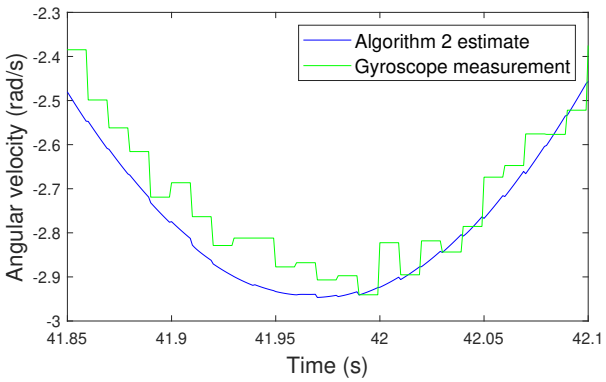

Fig. 8. Algorithm 2 - angular velocity estimate

inherent offset and drift errors are avoided in this manner. The same benefit can be expected also for the cart velocity since the filter offers also the estimate of this quantity.

IV. Conclusion

The paper proposes a systematic approach to observer design for the estimation of load tilt angles in crane control applications. The main result is a combination of the raw acceleration and angular rate data obtained from IMU with the predictive model governing the hoist-crane dynamics. This allows to mitigate the systematic errors caused by large transversal acceleration introduced by the load oscillations that affect the accelerometer sensor. Performance of the algorithm is demonstrated by means of an experimental benchmark. The proposed algorithm is compared in terms of performance with the standard solution for tilt angle estimation that does not consider neither the pendulum-on-cart dynamics nor the impact of rotational and translational acceleration distorting the gravitational acceleration sensing. Experimentally, it is shown that, when properly set, the proposed approach significantly outperforms the standard solution. Even with a suboptimal choice of the tuning parameter, an angle estimate of comparable quality can be obtained

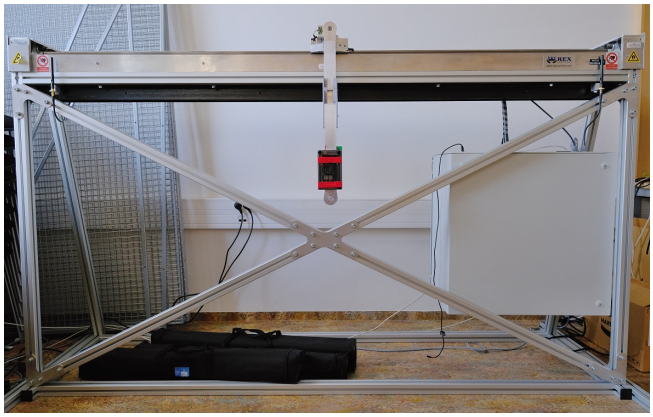

Fig. 9. Experimental setup - small-scale pendulum-on-cart model

with respect to the case of the standard algorithm with the best achievable setting. Future work will be directed towards extension of the algorithm to planar and 3D crane scenarios followed by full-scale plant experiments.

ACKNOWLEDGMENT

This work was supported from ERDF under project "Research and Development of Intelligent Components of Advanced Technologies for the Pilsen Metropolitan Area (InteCom)" No. CZ.02.1.010.00.017_048/0007267.

REFERENCES

[1] M. Goubej and M. Schlegel, "Feature-based parametrization of input shaping filters with time delays," *IFAC Workshop on time delay systems, Prague*, 2010.

[2] J. Vaughan, D. Kim, and W. Singhose, "Control of tower cranes with double-pendulum payload dynamics," *IEEE Transactions on Control Systems Technology*, vol. 18, no. 6, pp. 1345–1358, 2010.

[3] W. Singhose, D. Kim, and M. Kenison, "Input shaping control of double-pendulum bridge crane oscillations," *Journal of Dynamic Systems, Measurement, and Control*, vol. 130, no. 3, p. 034504, 2008.

[4] M. Giacomelli, F. Padula, L. Simoni, and A. Visioli, "Simplified input-output inversion control of a double pendulum overhead crane for residual oscillations reduction," *Mechatronics*, vol. 56, pp. 37 – 47, 2018.

[5] V. Helma and M. Goubej, "Vibration damping in gantry crane systems: Finite horizon optimal control approach," *24th IEEE Internetional Conference on Emerging Technologies and Factory Automation*, 2019.

[6] J. Vaughan, A. Karajgikar, and W. Singhose, "A study of crane operator performance comparing PD-control and input shaping," in *Proceedings of the 2011 American Control Conference*, June 2011, pp. 545–550.

[7] B. Yang and B. Xiong, "Application of LQR techniques to the anti-sway controller of overhead crane," *Advanced Materials Research*, vol. 139-141, pp. 1933–1936, 2010.

[8] M. Giacomelli, M. Faroni, D. Gorni, A. Marini, L. Simoni, and A. Visioli, "Model predictive control for operator-in-the-loop overhead cranes," in *2018 IEEE 23rd International Conference on Emerging Technologies and Factory Automation (ETFA)*, vol. 1, 2018, pp. 589–596.

[9] G. Kim and K. Hong, "Adaptive sliding-mode control of an offshore container crane with unknown disturbances," *IEEE/ASME Transactions on Mechatronics*, vol. 24, no. 6, pp. 2850–2861, 2019.

[10] N. Sun, Y. Fang, H. Chen, and B. He, "Adaptive nonlinear crane control with load hoisting/lowering and unknown parameters: Design and experiments," *IEEE/ASME Transactions on Mechatronics*, vol. 20, no. 5, pp. 2107–2119, 2015.

[11] X. He, W. He, J. Shi, and C. Sun, "Boundary vibration control of variable length crane systems in two-dimensional space with output constraints," *IEEE/ASME Transactions on Mechatronics*, vol. 22, no. 5, pp. 1952–1962, 2017.

[12] L. Ramli, Z. Mohamed, A. M. Abdullahi, H. Jaafar, and I. M. Lazim, "Control strategies for crane systems: A comprehensive review," *Mechanical Systems and Signal Processing*, vol. 95, pp. 1 – 23, 2017.

[13] Yong-Seok Kim, Han-Suk Seo, and Seung-Ki Sul, "A new anti-sway control scheme for trolley crane system," in *Conference Record of the 2001 IEEE Industry Applications Conference. 36th IAS Annual Meeting (Cat. No.01CH37248)*, vol. 1, 2001, pp. 548–552 vol.1.

[14] "ABB crane control solutions," https://new.abb.com/drives/media/crane-control-solutions, accessed: 2020-01-15.

[15] "SIEMENS SimoCrane sway control," https://mall.industry.siemens.com/mall/cs/cz/Catalog/Products/10218465, accessed: 2020-01-15.

[16] "Smartcrane anti-sway control," www.smartcrane.com, accessed: 2020-01-15.

[17] H. Kawai, Y. B. Kim, and Y. W. Choi, "Anti-sway system with image sensor for container cranes," *Journal of Mechanical Science and Technology*, vol. 23, pp. 2757–2765, 2009.

[18] G. O. Tysse, A. Cibicik, and O. Egeland, "Vision-based control of a knuckle boom crane with online cable length estimation," *IEEE/ASME Transactions on Mechatronics*, 2020.

[19] H. Kawai, Y. Kim, and Y. Choi, "Measurement of a container crane spreader under bad weather conditions by image restoration," *IEEE Transactions on Instrumentation and Measurement*, vol. 61, no. 1, pp. 35–42, 2012.

[20] Y. Kim, Y. Kim, Y. S. Jung, I. G. Jang, K. Kim, S. Kim, and B. M. Kwak, "Developing accurate long-distance 6-dof motion detection with one-dimensional laser sensors: Three-beam detection system," *IEEE Transactions on Industrial Electronics*, vol. 60, no. 8, pp. 3386–3395, 2013.

[21] Y. Kim, K. Hong, and S. Sul, "Anti-sway control of container cranes: Inclinometer, observer, and state feedback," *International Journal of Control, Automation, and Systems*, vol. 2, pp. 435–449, 2004.

[22] S. S. Enin, E. Y. Omelchenko, and A. V. Beliy, "Crane anti-sway control system with sway angle feedback," in *2018 International Conference on Industrial Engineering, Applications and Manufacturing (ICIEAM)*, 2018, pp. 1–5.

[23] L. D. Viet, "Crane sway reduction using coriolis force produced by radial spring and damper," *Journal of Mechanical Science and Technology*, vol. 29, pp. 973–979, 2015.

[24] W. Wang and P. G. Adamczyk, "Comparison of bingham filter and extended kalman filter in IMU attitude estimation," *IEEE Sensors Journal*, vol. 19, no. 19, pp. 8845–8854, 2019.

[25] X. Li, M. Chen, and L. Zhang, "Quaternion-based robust extended kalman filter for attitude estimation of micro quadrotors using low-cost mems," in *2016 35th Chinese Control Conference (CCC)*, July 2016, pp. 10 712–10 717.

[26] M. Ghobadi, P. Singla, and E. T. Esfahani, "Robust attitude estimation from uncertain observations of inertial sensors using covariance inflated multiplicative extended kalman filter," *IEEE Transactions on Instrumentation and Measurement*, vol. 67, no. 1, pp. 209–217, Jan 2018.

[27] M. Řezáč, "Inertial stabilization, estimation and visual servoing for aerial surveillance," Ph.D. dissertation, Czech Technical University in Prague, 2013.

[28] V. Šetka, O. Ježek, and R. Novickis, "Modular signal processing unit for motion control applications based on system-on-chip with FPGA," in *2019 24th IEEE International Conference on Emerging Technologies and Factory Automation (ETFA)*, 2019.

[29] "REXYGEN - programming automation devices without hand coding," www.rexygen.com, accessed: 2020-03-02.

[30] V. Šetka, R. Čecil, and M. Schlegel, "Triple inverted pendulum system implementation using a new ARM/FPGA control platform," *2017 18th International Carpathian Control Conference (ICCC)*, 2017.